

# Structure of a glutamate-receptor ligand-binding core in complex with kainate

Neali Armstrong<sup>\*†</sup>, Yu Sun<sup>\*†</sup>, Guo-Qiang Chen<sup>\*</sup>  
 & Eric Gouaux<sup>\*</sup>

<sup>\*</sup> Department of Biochemistry and Molecular Biophysics, Columbia University, 650 W. 168th Street, New York, New York 10032, USA

<sup>†</sup> These authors contributed equally to this work

**Ionotropic glutamate receptors (iGluRs) mediate excitatory synaptic transmission in vertebrates and invertebrates through ligand-induced opening of transmembrane ion channels. iGluRs are segregated into three subtypes according to their sensitivity to the agonists AMPA (α-amino-3-hydroxy-5-methyl-4-isoxazole propionic acid), kainate (a structural analogue of glutamate) or NMDA (N-methyl-D-aspartate) (Fig. 1). iGluRs are important in the development and function of the nervous system, are essential in memory and learning, and are either implicated in or have causal roles in dysfunctions ranging from Alzheimer's, Parkinson's and Huntington's diseases, schizophrenia, epilepsy and Rasmussen's encephalitis to stroke<sup>1,2</sup>. Development of iGluR agonists and antagonists has been hampered by a lack of high-resolution structural information. Here we describe the crystal structure of an iGluR ligand-binding region in a complex with the neurotoxin (agonist) kainate. The bilobed structure shows the determinants of receptor–agonist interactions and how ligand-binding specificity and affinity are altered by remote residues and the redox state of the conserved disulphide bond. The structure indicates mechanisms for allosteric effector action and for ligand-induced channel gating. The information provided by this structure will be essential in designing new ligands.**

The iGluR ligand-binding core is formed by polypeptide segments S1 and S2 (refs 3, 4). S1 includes ~150 residues amino-

terminal to the first transmembrane segment and S2 comprises the residues between membrane-associated segments 3 and 4 (Fig. 2). Definition of the S1S2 region as an autonomous ligand-binding core for all iGluRs is strengthened by site-directed mutagenesis and chimaeric and S1–S2 fusion experiments<sup>5</sup>. A construct in which the S1 and S2 regions of GluR4 are coupled by a 13-residue linker has pharmacological properties that are similar to those of the wild-type membrane-bound receptor<sup>4</sup>. We have previously developed methods to obtain large amounts of iGluR S1S2 protein from *Escherichia coli* and have generated new S1S2 constructs that form well-ordered crystals<sup>6</sup>.

We solved the structure of the rat GluR2 S1S2 ‘flop’ isoform bound to the non-desensitizing agonist kainate<sup>7</sup> by multiwavelength anomalous diffraction (MAD)<sup>8</sup> from crystals of the selenomethionine derivative. Of the 279 residues in the crystallized protein, there is corresponding electron density for 250 residues. The N-terminal 15 residues, 3 residues in loop 1, 9 amino acids in the S1–S2 linker region and the Gly–Ser dipeptide at the end of S2 are disordered in the crystal. Crystallographic statistics and views of the structure are shown in Table 1 and Figs 2 and 3.

The S1S2 structure has two α/β domains arranged in the shape of a kidney. It is 57 Å in length and has cross-sectional dimensions of 43 Å and 35 Å. The N terminus of the S1S2 construct is located in domain 1 and the carboxy terminus is at the end of helix K and is disulphide-bonded to domain 2. Domains 1 and 2 are composed mainly of polypeptide segments S1 and S2, respectively. However, S1 crosses over S2 and ends in domain 2, while the C terminus of S2 constitutes part of domain 1. Kainate is nestled between domains 1 and 2 and participates in multiple, primarily polar, contacts with residues from both domains. There are few, but significant, sequence relationships between GluR2 S1S2 and bacterial periplasmic-ligand binding proteins<sup>9</sup>; consistent with these relationships, the structure of the S1S2 construct is strikingly similar to that of the *E. coli* glutamine-binding protein (QBP)<sup>10</sup>.

Kainate binds in the interdomain crevice at the N termini of four α-helices; it induces domain closure and resistance to proteolysis<sup>6</sup>. The 2-carboxyl group forms essential interactions with the guanidinium group of Arg 485 and the main-chain NH group of Thr 480 of GluR2; mutation of Arg 485 to Lys or Ser at the corresponding sites in the homologous GluR4, NMDAR1 and NMDAR2B receptors and in chick kainate-binding protein (KBP) abolishes ligand-binding activity or agonist-induced opening of the ion channel<sup>11–13</sup>. Exploiting the macro dipole of helix F, the carboxyl methyl group forms hydrogen bonds with the NH groups of Ser 654 and Thr 655, the hydroxyl group of Thr 655, and two water molecules tethered to the peptide carbonyl oxygen of Ser 652 and the peptide nitrogen of Glu 705. Mutagenesis of Thr 268 to Ala in chick KBP (Thr 655 in GluR2) abolishes binding to <sup>3</sup>H-kainate<sup>13</sup>. Tyr 450 acts like a lid on top of the pyrrolidine ring and isopropenyl group of kainate, while the amino group is bound by the essential carboxylate of Glu 705, the carbonyl oxygen of Pro 478, and the sidechain hydroxyl of Thr 480. In NMDA receptors, an aspartate replaces the equivalent of Glu 705 in GluR2, perhaps to accommodate the ‘D’ stereocentre. The electrostatic potential of the ligand-binding site is highly negative and the net charge on kainate, AMPA and glutamate is –1. These apparently destabilizing electrostatic effects are compensated for by specific hydrogen bonds and salt links, and by helical dipole effects, as the N termini of four helices are located in the ligand site.

The isopropenyl group is partially exposed to solvent and projects into the interdomain crevice from underneath the Tyr 450 lid. The dearth of interactions with the isopropenyl group may be one reason why kainate binds relatively weakly to GluR2. Furthermore, the orientation of the isopropenyl group explains how ligands such as domoate, which have longer functional groups located at the 4 position of the pyrrolidine ring than does kainate, bind to the receptor. Four sequestered water molecules are next to the

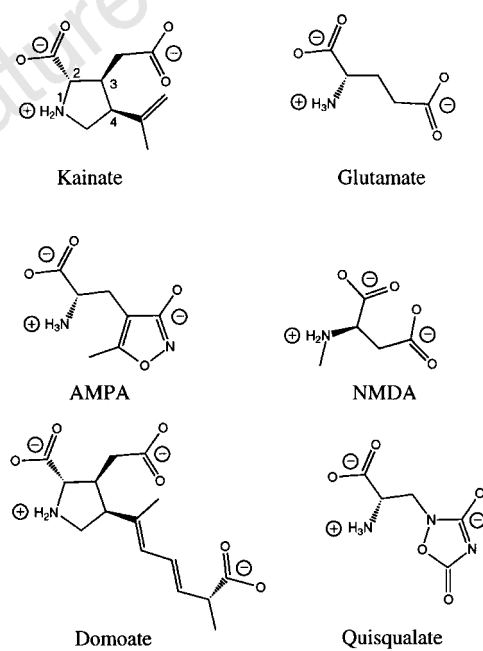


**Figure 1** Chemical structures of some iGluR agonists. The numbering of substituents on the pyrrolidine ring of kainate is as follows: nitrogen, 1; carboxylate, 2; carboxyl methyl, 3; and isopropenyl, 4.

isopropenyl and carboxyl methyl groups.

Ligand-binding affinity and specificity are altered by multidentate ligand–receptor interactions, which, in turn, induce and control domain separation. We suggest that binding of different agonists may result in variable degrees of domain closure. Binding of AMPA and glutamate to GluR2 S1S2 may allow more domain

closure than kainate. This is because AMPA and glutamate do not have the pyrrolidine ring and isopropenyl groups that together act like an interdomain wedge against the Tyr 450 lid. Fitting a model of AMPA onto the kainate structure shows that AMPA can supplant all of kainate's interactions, can accept an additional hydrogen bond through the isoxazole ring, and can allow greater domain closure.

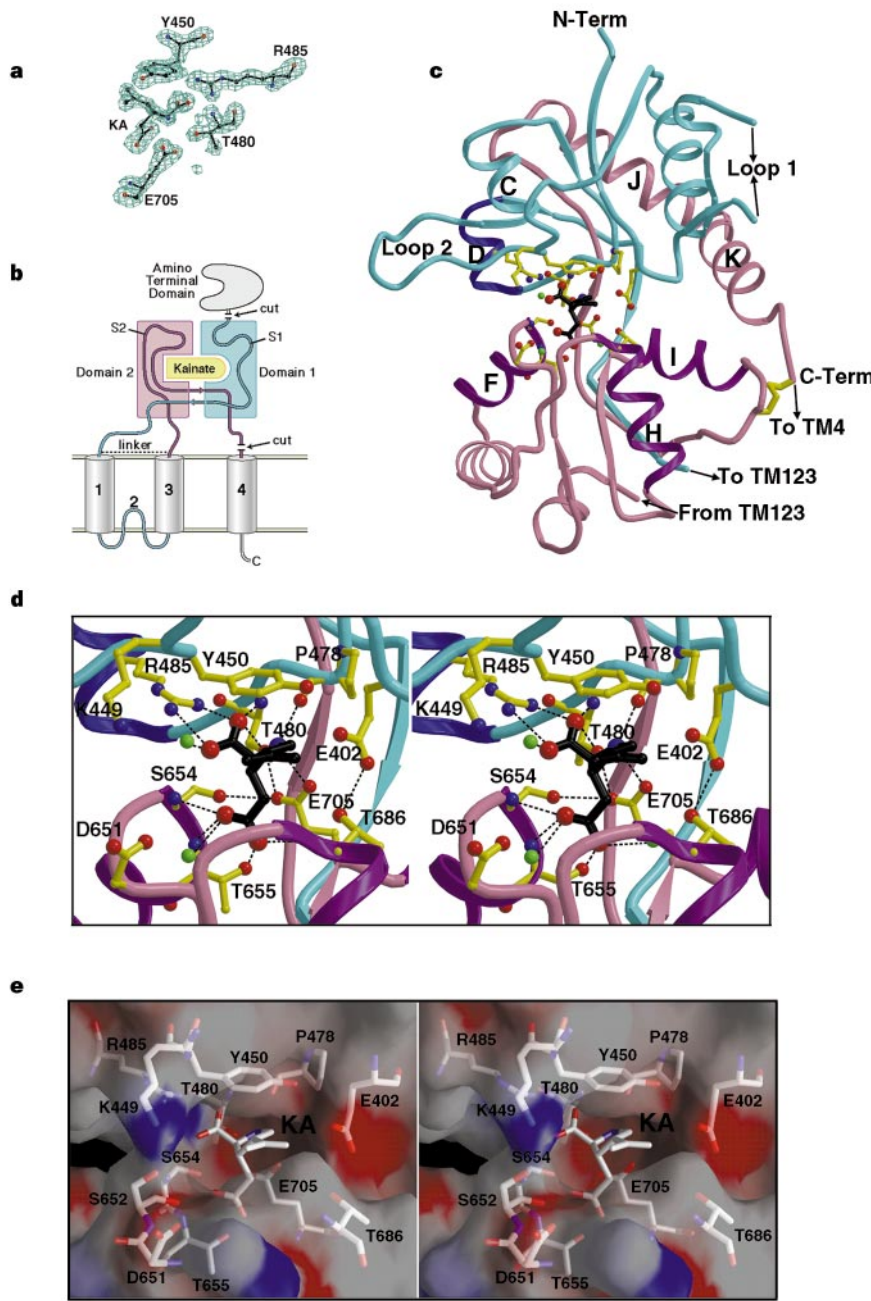


**Figure 2** Structure of the complex of GluR2 S1S2 and kainate. **a**, A  $F_o - F_c$  omit electron-density map of kainate and four selected ligand-binding residues, calculated using coefficients between 6.0 and 1.9 Å resolution and phases from the refined model. The map is contoured at 2.5  $\sigma$ . **b**, Domain structure of iGluRs, showing the S1 and S2 segments in turquoise and pink, respectively. 'Cut' and 'linker' denote the edges of the S1S2 construct. **c**, Ribbon representation of the S1S2 structure, with S1 and S2 coloured as in **b**. The N termini of helices D, F, H and I each contain a residue that either interacts with kainate (black ball-and-stick representation) or participates in interdomain contacts: Arg 485 projects into the kainate-binding site from helix D (dark purple); the backbone amides of Ser 654 and Thr 655 on helix F (light purple) interact with the carboxyl methyl group of

kainate; and helices H and I (light purple) contain residues Thr 686 and Glu 705. The disulphide bond between Cys 718 (helix I) and Cys 773 is shown in yellow. The C terminus of S1 is marked 'To TM123' and the N terminus of S2 is labelled 'From TM123'. Loops 1 and 2 protrude from the protein core by at least 10 Å and may be involved in domain–domain contacts. TM, transmembrane domain. **d**, Stereo view of the S1S2 region that encompasses kainate (black), showing interacting residues and residues that make interdomain contacts. The dashed lines indicate potential hydrogen bonds and ionic interactions between residues <3.2 Å apart. Water molecules are shown as green balls. **e**, Stereoview of the molecular surface, coloured by electrostatic potential; red, negative; blue, positive. Two regions of continuous molecular surface are formed on either side of kainate (KA).

Furthermore, the mode of ligand–receptor interaction seen in the complex of GluR2 S1S2 and kainate explains how glycine, which lacks an equivalent of kainate's carboxyl methyl group, can function as an NMDA-receptor agonist<sup>14</sup>: the amino and carboxyl groups bridge both domains, and promote domain closure and specific interdomain interactions.

Control of ligand affinity and specificity and of the kinetic properties of the ion channels also occurs through allosteric interactions and involves residue pairs on domain 1 and domain 2 that flank kainate (Glu 402–Thr 686 and Lys 449–Asp 651, Ser 652; Fig. 2). The residue at position 686 of GluR2 in the kainate receptors GluR5 (Ser) and GluR6 (Asn) is important in determining sensitivity to AMPA and the rate of deactivation by domoate<sup>15</sup>. In the sulphate-binding protein, disruption of similar interdomain interactions significantly increases the  $K_d$  value and  $k_{off}$  rate for sulphate<sup>16</sup>. As seen in GluR2 S1S2, Glu 402 forms a hydrogen bond with the hydroxyl group of Thr 686. Although Lys 449 (which is in domain 1) does not contact residues on domain 2 directly, it is only  $\sim 4$  Å from Asp 651 and Ser 652. If further domain closure were to occur upon glutamate or AMPA binding, Lys 449 could participate in an interdomain salt link or hydrogen bond. In fact, when the equivalent lysine in GluR1 is mutated to glutamine, the effector concentrations for half-maximal response (EC<sub>50</sub> values) for glutamate and AMPA increase; there is no effect on the EC<sub>50</sub> for kainate<sup>17</sup>.

A comparison of the kainate–S1S2 structure and the QBP–glutamine structure (Fig. 3)<sup>10</sup> supports the theory that the GluR2 S1S2 domains may undergo further domain closure. When domain 1 of S1S2 is superimposed on domain 1 of the closed form of QBP, a rotation of 21° around an axis located between the domains is needed to superimpose domains 2. When the open form of QBP is used as the template, a rotation of 32° is required to fit domain 2 of S1S2 on domain 2 of QBP. Compared with the open and closed forms of QBP, the GluR2 S1S2 complex containing kainate is intermediate with respect to domain closure. To determine whether further domain closure could occur in the presence of different ligands, such as AMPA, we independently fit domains 1 and 2 of S1S2 to the closed form of QBP by creating two interdomain breaks in the polypeptide chain. In the resulting S1S2 model there were only a few steric clashes, involving Lys 449 and Ser 652, and Glu 402 and Met 708. Thus, further domain closure is possible if a few residues and associated elements of the main chain undergo conformational changes.

Redox modulation of NMDA-receptor activity, in which disulphide-reducing agents increase NMDA-gated currents and oxidizing agents decrease the currents<sup>18</sup>, may be understood in terms of the conserved interdomain disulphide bond between Cys 718 and Cys 773. Redox control of the receptor may occur by making domain closure more difficult (in the oxidized state) or easier (in the reduced state). By analogy with QBP, in domain-closed forms of the receptor the distance between the cysteine residues is larger than in more open forms and thus cleavage of the disulphide bond by reduction or mutagenesis increases ligand-binding affinity or ligand-induced current by allowing domain closure<sup>19</sup>. Domain movement in the oxidized state probably also involves contraction and extension of the polypeptide chain at the end of helix K.

Sequence alignment of regions of iGluRs that include domains corresponding to the S1S2 construct of GluR2 shows that all iGluRs have a common core, indicates the site of allosteric effector action, and maps the location of the flip/flop residues encoded by separate exons<sup>7</sup>. All seven residues that make direct interactions with kainate in the GluR2 S1S2 complex are identical or conservatively substituted among the members of the four iGluR subfamilies, which include the kainate-binding proteins, even though the overall degree of sequence identity between iGluRs is <10% (Fig. 4). All four flip/flop sites in this GluR2 S1S2 construct, in addition to the RNA-editing site, are located on the solvent-exposed surface of helices J and K. The flip (Ser) and flop (Asn) variants at position 754 of GluR2 have differential allosteric responses to cyclothiazide. Kainate receptors, which contain a Gln at this position, are insensitive to cyclothiazide. Mutation of Ser 750 to Gln in the AMPA receptor GluR1 (position 754 in GluR2) abolishes modulation by cyclothiazide, whereas introduction of Ser at the equivalent site in the kainate receptor GluR6 confers sensitivity to cyclothiazide<sup>20</sup>. The clustering of Asn 754, Leu 748 and Leu 751 indicates that this

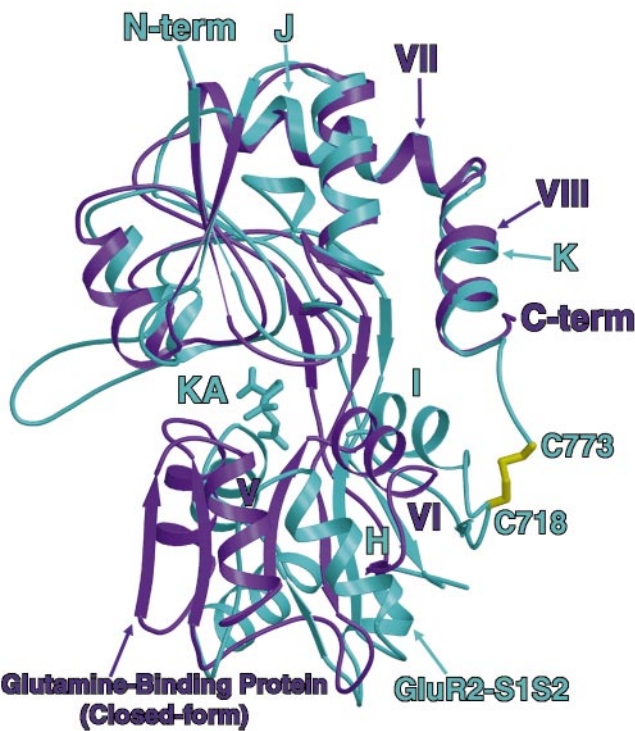


**Figure 3** Superposition of the complex of GluR2 S1S2 and kainate (KA) with the closed form of QBP<sup>10</sup>. Helices I, VII and VIII from QBP were fit to helices B, J and K, respectively, of GluR2 S1S2; of these, helices VII, VIII, J and K are labelled. Following this superposition, the root mean square (r.m.s.) deviations of  $\alpha$ -carbon positions is 1.0 Å for the atoms fit, 1.6 Å for domain 1, 8.5 Å for domain 2 and 5.5 Å for both domains. Subsequent fitting of domains 2 from QBP and GluR2 S1S2 gives r.m.s. deviations of  $\alpha$ -carbon positions of 2.1 Å for domain 2, 6.6 Å for domain 1 and 5.2 Å overall.

**Table 1** Refinement statistics

Resolution (Å)	Reflections (N)	$R^*$ (%)	$R_{free}^†$ (%)	Average $B$ -value			r.m.s. deviations			
				Overall	Main	Ligand	Bonds		Angles	
							Bonds	Angles	Bonds	Angles
6.0–1.9	19,483	21.6	27.3	18.86	17.53	11.07	0.011 Å	1.483°	2.5	3.5

The model included 250 residues, 175 water molecules, 1 kainate molecule and 2,068 atoms.

\*  $R$ -factor =  $(\sum |F_o| - |F_c|)/\sum |F_o|$ , where  $F_o$  and  $F_c$  denote observed and calculated structure factors, respectively, and summation extends over all observed reflections.

† 8% of the structure factors between 6.0 and 1.9 Å were set aside to calculate the  $R$ -free factor.

surface is the site of effector action and that, because of its hydrophobic character, this surface is probably involved in intra-subunit or intersubunit contacts; in other words, cyclothiazide, aniracetam and thiocyanate<sup>21</sup> may function by perturbing interfaces that are >25 Å from the ligand-binding site. The agonist-like effects of autoantibodies implicated in Rasmussen's encephalitis<sup>2</sup> also act at a substantial distance from the ligand-binding site: on the basis of the S1S2 structure, the epitope(s) are located just upstream of the start of S1, near helix J.

This is, to our knowledge, the first high-resolution structure of an iGluR ligand-binding core, and it revealed the following unexpected facts. First, the ligand-binding site of GluR2 has a negative electrostatic potential. Second, the carboxyl methyl group of kainate is neutralized by hydrogen bonds from the N terminus of helix F. Third, the binding of kainate to GluR2 S1S2 induces an intermediate degree of domain closure relative to QBP's open and closed

conformations; this degree of closure corresponds to the open, non-desensitized state of the intact receptor. Fourth, some of the residues that mediate agonist specificity and channel dynamics form interdomain contacts. Finally, the exposed face of helix J is probably a site of binding of allosteric effectors and of domain-domain contacts. □

## Methods

**Crystallization and data collection.** We expressed, purified, characterized and crystallized the GluR2 S1S2 construct as described<sup>6</sup>. The space group and unit-cell dimensions for the S1S2–kainate co-crystals are  $P_2_1$ , and  $a = 42.22 \text{ \AA}$ ,  $b = 63.07 \text{ \AA}$ ,  $c = 46.32 \text{ \AA}$  and  $\beta = 92.99^\circ$ . The methionine and selenomethionine (SeMet) crystals were isomorphous. Diffraction data sets were collected at the NSLS X4a and CHESS F-2 beamlines from selenomethionine crystals that were flash-cooled in liquid nitrogen and maintained in a stream of nitrogen gas at  $-150^\circ\text{C}$ . Before cooling, the crystals were soaked in the crystallization reservoir

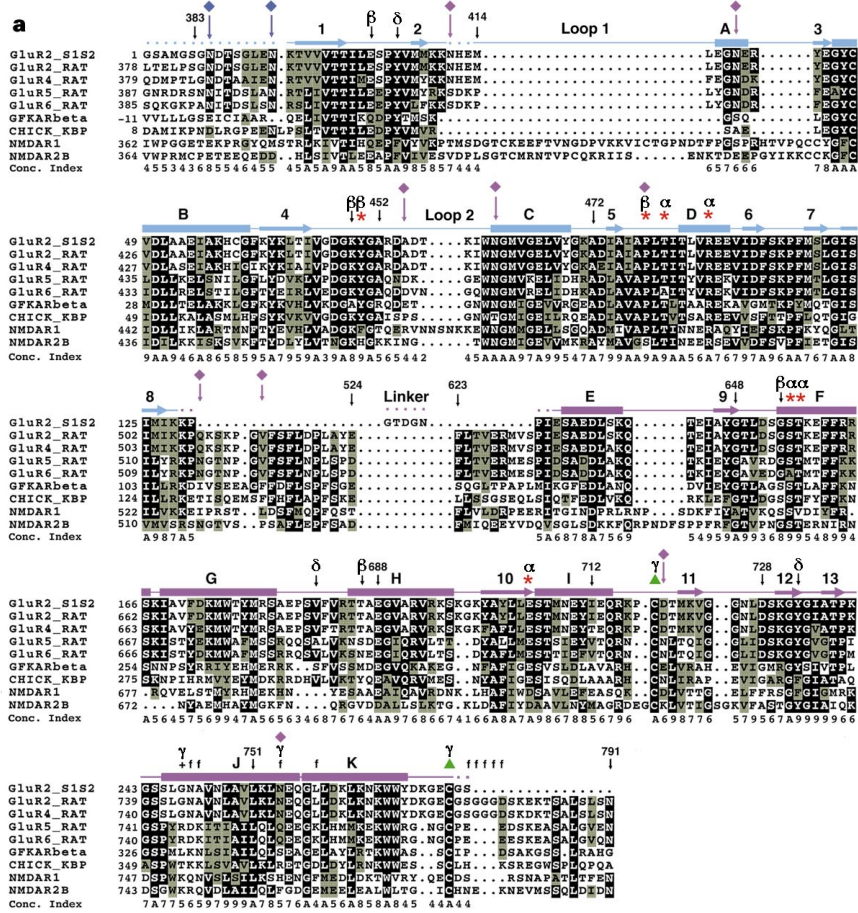


**Figure 4** Sequence identity between iGluRs. **a**, Multiple sequence alignment of selected AMPA, kainate and NMDA receptors and kainate-binding proteins. Residues are defined as not conserved (conservation index of 0) through to moderately well-conserved (index of 8) and highly conserved (index of A).  $\alpha$ -Helices (rectangles) and  $\beta$ -strands (arrows) are drawn above the sequences, with colouring as in Fig. 2; dotted lines indicate regions for which there is no electron density available for the main chain. Ligand-binding residues are indicated by red stars. The disulphide-bond-forming cysteines are marked by green triangles. Flip/flop residues of GluR2 are delineated by 'f' and the RNA-editing site by '+'. Glycosylation sites in GluR1 are labelled with diamonds, which are magenta for engineered sites and blue for natural sites<sup>28</sup>. Functionally important residues are defined as follows:  $\alpha$ , residues interacting with all agonists;  $\beta$ , residues that interact with specific ligands;  $\gamma$ , residues involved in the regulation of ligand binding and the kinetic properties of the channel;  $\delta$ , residues that do not interact directly with the ligand but may be important for the structure of the binding pocket. Sequences are numbered according to the predicted mature polypeptide. **b**, The degree of conservation (0, white, to A, black) is mapped onto each residue position of GluR2 S1S2. The four flip/flop sites (Asn 744, Ala 745, Asn 754 and Leu 758; shown in magenta) and the Arg/Gly RNA-editing site (Gly 743) are located on helices J and K. Residue Asn 754 (flip, Gly; flop, Asn) is involved in the allosteric responses to cyclothiazide<sup>20</sup>. The Arg/Gly RNA-editing site (Gly 743) influences the rate of recovery from desensitization<sup>29</sup>. **c**, Solvent-accessible surface of GluR2 S1S2, in the same orientation as in **b**. Hydrophobic residues (Ala, Val, Leu, Ile, Met, Pro, Phe, Tyr and Trp) are purple; residues with a conservation index of 9 or A are green; exposed and conserved hydrophobic residues are black. A cylindrical depression, ~3.5 Å in diameter and 4.0 Å deep, is located at the Arg/Gly RNA-editing site.

residues that do not interact directly with the ligand but may be important for the structure of the binding pocket. Sequences are numbered according to the predicted mature polypeptide. **b**, The degree of conservation (0, white, to A, black) is mapped onto each residue position of GluR2 S1S2. The four flip/flop sites (Asn 744, Ala 745, Asn 754 and Leu 758; shown in magenta) and the Arg/Gly RNA-editing site (Gly 743) are located on helices J and K. Residue Asn 754 (flip, Gly; flop, Asn) is involved in the allosteric responses to cyclothiazide<sup>20</sup>. The Arg/Gly RNA-editing site (Gly 743) influences the rate of recovery from desensitization<sup>29</sup>. **c**, Solvent-accessible surface of GluR2 S1S2, in the same orientation as in **b**. Hydrophobic residues (Ala, Val, Leu, Ile, Met, Pro, Phe, Tyr and Trp) are purple; residues with a conservation index of 9 or A are green; exposed and conserved hydrophobic residues are black. A cylindrical depression, ~3.5 Å in diameter and 4.0 Å deep, is located at the Arg/Gly RNA-editing site.

solution supplemented with ~20% (*w/v*) PEG 400. After using the SeMet crystals to obtain a fluorescence curve as a function of the incident X-ray energy, we collected data sets at 12659.0 eV, 12663.5 eV, 12800.0 eV and 12630.0 eV using inverse-beam geometry. The data sets from the R-Axis4 detector at NSLS X4a and the Quantum 4 detector at CHESS were processed using DENZO and SCALEPACK<sup>22</sup>.

**Structure determination.** Determination and refinement of the selenium sites and initial phase calculations were done using the program SOLVE (from T. Terwilliger; see <http://www.solve.lanl.gov> and references therein). Density modification that included solvent flattening and histogram matching, using the program DM<sup>23</sup>, improved the quality of the electron-density maps calculated using either the NSLS or the CHESS data. However, the maps derived from the NSLS or CHESS data were mediocre and could not be used to trace more than a small fraction of the polypeptide chain. Substantial improvement of the electron-density maps resulted from combination of the NSLS and CHESS phases using the program SIGMAA<sup>24</sup> and use of  $|F_o|$  derived from a selenomethionine data set collected at home (2.3 Å resolution, CuK $\alpha$  X-rays) and MAD-combined phases. Phase combination in reciprocal space and map averaging in real space produced similar results. Using experimental maps calculated at 2.5 and 2.3 Å resolution, we built a structure comprising 86% of the 279 residues by using the program O (ref. 25). After the first round of Powell minimization and *B*-factor refinement using XPLOR<sup>26</sup>, the conventional *R*-value was 0.322 and the *R*-free value was 0.389. At this point, we used native data measured to 1.9 Å resolution for the remainder of the refinement and model building until the *R* values converged, beginning at 2.3 Å resolution and gradually including higher-resolution terms. We then built kainate into an 'omit' map calculated using phases from the refined model and  $F_o - F_c$  coefficients, and carried out another round of Powell minimization and *B*-factor refinement. Unless otherwise noted, CCP4 programs<sup>27</sup> were used for crystallographic calculations. There is either no or weak electron density for the following side chains and they have therefore been omitted from the structure and replaced by Ala: Lys 393, Lys 410, Glu 416, Lys 434, Asp 456, Leu 483, Lys 493, Glu 634, Ser 635, Glu 637, Lys 641, Gln 642, Thr 643, Arg 661, Lys 663, Glu 678, Lys 695, Lys 697 and Ser 741.

Received 14 August; accepted 18 September 1998.

- Hollmann, M. & Heinemann, S. Cloned glutamate receptors. *Annu. Rev. Neurosci.* **17**, 31–108 (1994).
- Rogers, S. W. *et al.* Autoantibodies to glutamate receptor GluR3 in Rasmussen's encephalitis. *Science* **265**, 648–651 (1994).
- Stern-Bach, Y. *et al.* Agonist selectivity of glutamate receptors is specified by two domains structurally related to bacterial amino acid-binding proteins. *Neuron* **13**, 1345–1357 (1994).
- Kuusinen, A., Arvola, M. & Keinänen, K. Molecular dissection of the agonist binding site of an AMPA receptor. *EMBO J.* **14**, 6327–6332 (1995).
- Paas, Y. The macro- and microarchitectures of the ligand-binding domain of glutamate receptors. *Trends Neurosci.* **21**, 117–125 (1998).
- Chen, G.-Q., Sun, Y., Jin, R. & Gouaux, E. Probing the ligand binding domain of the GluR2 receptor by proteolysis and deletion mutagenesis defines domain boundaries and yields a crystallizable construct. *Protein Sci.* (in the press).
- Sommer, B. *et al.* Flip and flop: a cell-specific functional switch in glutamate-operated channels of the CNS. *Science* **249**, 1580–1585 (1990).
- Hendrickson, W. A. Determination of macromolecular structures from anomalous diffraction of synchrotron radiation. *Science* **254**, 51–58 (1991).
- Nakanishi, N., Shneider, N. A. & Axel, R. A family of glutamate receptor genes: evidence for the formation of heteromultimeric receptors with distinct channel properties. *Neuron* **5**, 569–581 (1990).
- Sun, Y.-J., Rose, J., Wang, B.-C. & Hsiao, C.-D. The structure of glutamine-binding protein complexed with glutamine at 1.94 Å resolution: comparisons with other amino acid binding proteins. *J. Mol. Biol.* **278**, 219–229 (1998).
- Keinänen, K., Arvola, M., Kuusinen, A. & Johnson, M. Ligand recognition in glutamate receptors: insights from mutagenesis of the soluble  $\alpha$ -amino-3-hydroxy-5-methyl-4-isoxazole propionic acid (AMPA)-binding domain of glutamate receptor type D (GluR-D). *Biochem. Soc. Trans.* **25**, 835–838 (1997).
- Laube, B., Hirai, H., Sturgess, M., Betz, H. & Kuhse, J. Molecular determinants of agonist discrimination by NMDA receptor subunits: analysis of the glutamate binding site on the NR2B subunit. *Neuron* **18**, 493–503 (1997).
- Paas, Y., Eisenstein, M., Medeville, F., Teichberg, V. I. & Devilliers-Thiéry, A. Identification of the amino acid subsets accounting for the ligand binding specificity of a glutamate receptor. *Neuron* **17**, 979–990 (1996).
- Hirai, H., Kirsch, J., Laube, B., Betz, H. & Kuhse, J. The glycine binding site of the N-methyl-D-aspartate receptor subunit NR1: identification of novel determinants of co-agonist potentiation in the extracellular M3-M4 loop region. *Proc. Natl. Acad. Sci. USA* **93**, 6031–6036 (1996).
- Swanson, G. T., Gereau, R. W. IV, Green, T. & Heinemann, S. F. Identification of amino acid residues that control functional behavior in GluR5 and GluR6 kainate receptors. *Neuron* **19**, 913–926 (1997).
- Jacobson, B. L., He, J. J., Lemon, D. D. & Quijano, F. A. Interdomain salt bridges modulate ligand-induced domain motion of the sulfate receptor protein for active transport. *J. Mol. Biol.* **223**, 27–30 (1992).
- Li, F., Owens, N. & Verdoorn, T. A. Functional effects of mutations in the putative agonist binding region of recombinant  $\alpha$ -amino-3-hydroxy-5-methyl-4-isoxazolepropionic acid receptors. *Mol. Pharmacol.* **47**, 148–154 (1995).
- Aizenman, E., Lipton, S. A. & Loring, R. H. Selective modulation of NMDA responses by reduction and oxidation. *Neuron* **2**, 1257–1263 (1989).

- Sutcliffe, M. J., Wo, Z. G. & Oswald, R. E. Three-dimensional models of non-NMDA glutamate receptors. *Biophys. J.* **70**, 1575–1589 (1996).
- Partin, K. M., Bowie, D. & Mayer, M. L. Structural determinants of allosteric regulation in alternatively spliced AMPA receptors. *Neuron* **14**, 833–843 (1995).
- Partin, K. M., Fleck, M. W. & Mayer, M. L. AMPA receptor flip/flop mutants affecting deactivation, desensitization, and modulation by cyclothiazide, aniracetam, and thiocyanate. *J. Neurosci.* **16**, 6634–6647 (1996).
- Otwinsky, Z. & Minor, W. Processing of X-ray diffraction data collected in oscillation mode. *Methods Enzymol.* **276**, 307–326 (1997).
- Cowtan, K. D. & Main, P. Phase combination and cross validation in iterated density-modification calculations. *Acta Crystallogr. D* **42**, 43–48 (1996).
- Read, R. J. Model phases: probabilities and bias. *Methods Enzymol.* **277**, 110–128 (1997).
- Jones, T. A. & Kjeldgaard, M. Electron-density map interpretation. *Methods Enzymol.* **277**, 173–208 (1997).
- Brünger, A. T. *X-PLOR. Version 3.1. A System for X-ray Crystallography and NMR* 1–382 (Yale Univ. Press, New Haven, 1992).
- Collaborative Computational Project Number 4. The CCP4 suite: programs for protein crystallography. *Acta Crystallogr. D* **50**, 760–763 (1994).
- Hollmann, M., Maron, C. & Heinemann, S. N-Glycosylation site tagging suggests a three transmembrane domain topology for the glutamate receptor GluR1. *Neuron* **13**, 1331–1343 (1994).
- Lomeli, H. *et al.* Control of kinetic properties of AMPA receptor channels by nuclear RNA editing. *Science* **266**, 1709–1713 (1994).

**Acknowledgements.** We thank C. Lima and other members of the Hendrickson laboratory for assistance; J. Lidestri for maintenance of the X-ray laboratory at Columbia University; A. Karlin, J. Javitch and M. Akabas for advice; S. Heinemann and M. Hartley for glutamate-receptor clones; C. Ogata for help with MAD data collection at NSLS X4a; T. Terwilliger for advice on the use of Solve; and W. Minor and Z. Otwinsky for a new version of the HKL suite of programs. Extra MAD data were collected at the Cornell High Energy Synchrotron Source (CHESS), which is supported by the NSF, using the Macromolecular Diffraction at CHESS (MacCHESS) facility, which is supported by an award from the NIH. N.A. was supported by an NIH Ophthalmology training grant. E.G. is an NSF Young Investigator and the recipient of an Alfred P. Sloan Research Fellowship.

Correspondence and requests for materials should be addressed to E.G. (e-mail: jeg52@columbia.edu). The GluR2 S1S2 coordinates have been deposited with the Protein Data Bank and have accession code 1gr2.

## Chromatin deacetylation by an ATP-dependent nucleosome remodelling complex

Jeffrey K. Tong\*, Christian A. Hassig\*, Gavin R. Schnitzler†, Robert E. Kingston† & Stuart L. Schreiber\*

\* Howard Hughes Medical Institute, Departments of Chemistry and Chemical Biology, Molecular and Cellular Biology, Harvard University, 12 Oxford Street, Cambridge, Massachusetts 02138, USA

† Department of Molecular Biology, Massachusetts General Hospital, Boston, Massachusetts 02114, USA

The dynamic assembly and remodelling of eukaryotic chromosomes facilitate fundamental cellular processes such as DNA replication and gene transcription. The repeating unit of eukaryotic chromosomes is the nucleosome core, consisting of DNA wound about a defined octamer of histone proteins<sup>1</sup>. Two enzymatic processes that regulate transcription by targeting elements of the nucleosome include ATP-dependent nucleosome remodelling and reversible histone acetylation<sup>2,3</sup>. The histone deacetylases, however, are unable to deacetylate oligonucleosomal histones *in vitro*<sup>4</sup>. The protein complexes that mediate ATP-dependent nucleosome remodelling and histone acetylation/deacetylation in the regulation of transcription were considered to be different, although it has recently been suggested that these activities might be coupled<sup>5</sup>. We report here the identification and functional characterization of a novel ATP-dependent nucleosome remodelling activity that is part of an endogenous human histone deacetylase complex. This activity is derived from the CHD3 and CHD4 proteins which contain helicase/ATPase domains found in SWI2-related chromatin remodelling factors, and facilitates the deacetylation of oligonucleosomal histones *in vitro*. We refer to this complex as the nucleosome remodelling and deacetylating (NRD) complex. Our results establish a physical and functional link between the distinct chromatin-modifying activities of histone deacetylases and nucleosome remodelling proteins.